Mixing Behaviors of Wet Granular Materials in Gas Fluidized Bed Systems

Eldin Wee Chuan Lim and Reginald Beng Hee Tan
Dept. of Chemical and Biomolecular Engineering, National University of Singapore, Singapore, 117576 Singapore

Zongyuan Xiao
Dept. of Chemical and Biochemical Engineering, College of Chemistry and Chemical Engineering, Xiamen University, Xiamen 361005, P.R. China

DOI 10.1002/aic.14177
Published online July 5, 2013 in Wiley Online Library (wileyonlinelibrary.com)

The discrete element method combined with computational fluid dynamics was coupled with a capillary liquid bridge force model for computational studies of mixing behaviors in gas fluidized bed systems containing wet granular materials. Due to the presence of strong capillary liquid bridge forces between wet particles, relative motions between adjacent particles were hindered. There was a high tendency for wet particles to form large aggregates within which independent motions of individual particles were limited. This resulted in much lower mixing efficiencies in comparison with fluidization of dry particles. Capillary liquid bridge forces were on average stronger than both fluid drag forces and particle–particle collision forces and this accounted for the difficulty with which individual particles could be removed and transferred between aggregates. Such exchange of particles between aggregates was necessary for mixing to occur during fluidization of wet granular materials but required strong capillary liquid bridge forces to be overcome.
 AIChE J, 59: 4058–4067, 2013
Keywords: mixing, wet granular materials, fluidized beds, discrete element method, computational fluid dynamics

Introduction

Gasification is the process of converting carbonaceous materials into gases, such as carbon monoxide and hydrogen through high-temperature reactions with steam or oxygen. The reaction is usually carried out in a fluidized bed reactor in the presence of fine catalyst particles and at high temperatures. Recent studies have suggested that the use of mixtures of carbon sources for gasification reactions may result in synergistic effects that may lead to higher reaction yields and lower production of the by-product known as tar in such processes. In such co-gasification processes, fluidization of at least two different types of solid particles in a fluidized bed reactor is necessary. Due to differences in sizes and material properties of the different types of solid particles, the fluidization behavior is expected to be different and much more complex than single-species fluidization. This has strong implications for actual co-gasification operations as good contacting and mixing between the various types of particles is essential for efficient chemical reactions. In addition, feedstocks for co-gasification reactions may include various types of solid materials that contain large quantities of moisture such as low rank coal, horticultural waste, domestic waste or sewage sludge. As such, a good understanding of the fluidizing and mixing behaviors of wet solid particles will be instrumental for the eventual design of industrial fluidized bed systems for carrying out integrated mixing–drying operations for feedstocks of co-gasification processes that comprise mixtures of wet granular materials.

Although several studies of solids mixing in fluidized bed systems have been reported in the research literature, mixing behaviors of wet granular materials during fluidization does not seem to have been adequately addressed to date. Rhodes et al.[1] examined the usefulness of the discrete element method (DEM) for studying solids mixing in gas fluidized beds and showed that gas velocity and particle properties were important parameters influencing solids mixing in bubbling fluidized beds. Feng et al.[2] reported a numerical study of segregation and mixing of binary mixtures of particles in a gas fluidized bed via the approach of combining the DEM with computational fluid dynamics (CFD). They subsequently extended their study to investigate the effects of gas velocity on mixing behaviors under partially and fully fluidized conditions.[3] Dahl and Hrenya[4] also applied a similar Eulerian–Lagrangian model based on DEM and CFD to investigate segregation behavior in gas fluidized bed systems with continuous particle size distributions. The mixing behaviors of solid particles in other fluidized bed systems of interest, such as inclined fluidized beds[5] as well as rotating fluidized beds,[6] have similarly been examined by various researchers in recent years. Apart from the Eulerian–Lagrangian or CFD–DEM approach, the Eulerian–Eulerian approach based on a two-fluid model had also been applied for studies of mixing behaviors in fluidized bed systems. Cooper and Coronella[7] used such an approach to simulate a binary fluidized bed and investigate the effects of gas

Correspondence concerning this article should be addressed to E. W. C. Lim at chelwce@nus.edu.sg.

velocity, maximum packing fraction and solids composition on extent of mixing. The multifluid Eulerian model incorporating the kinetic theory of granular flow has also been applied by several researchers for studies of mixing and segregation behaviors in fluidized bed systems containing binary mixtures of particles differing in sizes or densities.[8–11] More recently, Gui and Fan[12] demonstrated the method of coupling DEM with large eddy simulation (LES) for studies of mixing of monodispersed particles with identical densities in bubbling fluidized beds.

In addition to modeling and computational studies, experimental investigations of mixing behaviors in gas fluidized bed systems have also been reported by many researchers. Du et al.[13] examined gas and solids mixing in bubbling and turbulent fluidized beds using helium and phosphor tracer techniques as well as electrical capacitance tomography. The dispersion behaviors of solids in the axial and radial directions were analyzed for the bubbling, turbulent and fast fluidization regimes. Wormsbecker et al.[14] applied a core sampling technique to study segregation patterns in a conical fluidized bed of dry pharmaceutical granulate with a continuous, bimodal particle size distribution. Joseph et al.[15] conducted axial and radial segregation measurements of species segregation for binary Geldart group B mixtures of particles differing in size and/or density by frozen bed sectioning techniques. Experimental studies have also been conducted on mixing behaviors in spouting fluidized beds,[16] nanoagglomerate fluidized beds,[17] beds composed of biomass-sand mixtures,[18] as well as bubbling fluidized beds containing Geldart group B particles with continuous, Gaussian or log-normal size distributions.[19]

Despite the potential importance of fluidized bed mixers and dryers for preprocessing of feedstocks comprising mixtures of wet granular materials for co-gasification operations, studies of mixing behaviors of wet solids in gas fluidized bed systems have been limited. One of the first computational studies in this area was reported by Mikami et al.[20] who applied the CFD–DEM approach for simulations of wet powder fluidization and observed that the minimum fluidizing velocity for wet particles was higher than that for dry particles. Jain et al.[21] showed that the CFD–DEM approach coupled with a capillary liquid bridge force model was useful for characterizing differences in minimum fluidization velocities of dry and wet particles. Tardos and Pfeffer[22] demonstrated experimentally the occurrence of agglomeration of particles due to the formation of new species during a chemical reaction that occurred on the surface of the particles leading to defluidization. Wormsbecker and Pugsley[23] conducted experiments to demonstrate the effects of liquid bridging on fluidization behaviors of porous pharmaceutical granules and observed that the granules exhibited Geldart C type fluidization behaviors at high moisture contents and Geldart B type behaviors otherwise.

Studies of mixing behaviors of dry or wet granular materials in gas fluidized bed systems that have been reported in the literature to date, such as the work by Jain et al.[21] reviewed above, have focused largely on the kinematics aspects of fluidization and mixing behaviors. These do not provide deeper insights to the underlying mechanisms of the mixing behaviors that gave rise to such observations as low mixing efficiencies of wet granular materials in gas fluidized bed systems. To gain deeper insights to the fundamental mechanisms responsible for such fluidization and mixing behaviors, considerations of the dynamics aspects of fluidization and mixing are essential. In other words, analyses of the various forces present within the fluidized bed systems during fluidization and mixing are required. In the present study, the conventional CFD–DEM model was coupled with a capillary liquid bridge force model to investigate the mixing behaviors of dry and wet solid particles in gas fluidized bed systems. Mixing efficiencies were compared quantitatively via a mixing index and dynamic force data at the scale of individual particles were extracted from the simulations conducted and analyzed with a view towards advancing current understanding of the mechanisms involved in mixing of wet granular materials during fluidization processes. In the following section, the computational model and physical system of interest to the present study will be described. The simulation results obtained for the various physical conditions considered in this study will then be discussed and a summary of the conclusions derived will be presented in the Conclusions section of this article.

Computational Model

Discrete element method

The DEM was developed by Cundall and Strack[24] for modeling the behavior of assemblies of discs and spheres. With the advent of computational power in recent years, it has been applied for studies of various types of multiphase flow systems.[25–31] In this section, a brief description of the method and corresponding governing equations will be presented.

The governing equations in DEM for describing translational and rotational motions of individual solid particles are basically Newton's laws of motion

$$m_i \frac{d\mathbf{v_i}}{dt} = \sum_{j=1}^{N} \left(\mathbf{f_{c,ij}} + \mathbf{f_{d,ij}}\right) + \mathbf{f_{f,i}} + \mathbf{f_{cap,ij}} + m_i \mathbf{g} \tag{1}$$

$$I_i \frac{d\omega_\mathbf{i}}{dt} = \sum_{j=1}^{N} \mathbf{T_{ij}} \tag{2}$$

where m_i and $\mathbf{v_i}$ are the mass and velocity of the ith particle, respectively, N is the number of particles in contact with the ith particle, $\mathbf{f_{c,ij}}$ and $\mathbf{f_{d,ij}}$ are the contact and viscous contact damping forces, respectively, $\mathbf{f_{f,i}}$ is the fluid drag force, $\mathbf{f_{cap,ij}}$ is the capillary liquid bridge force between wet particles, I_i is the moment of inertia of the ith particle, $\boldsymbol{\omega_i}$ is its angular velocity and $\mathbf{T_{ij}}$ is the torque arising from contact forces which causes the particle to rotate.

Contact and damping forces were calculated by applying a linear spring-and-dashpot model as closure. The normal ($\mathbf{f_{cn,ij}}$, $\mathbf{f_{dn,ij}}$) and tangential ($\mathbf{f_{ct,ij}}$, $\mathbf{f_{dt,ij}}$) components of the contact and damping forces were calculated as follows

$$\mathbf{f_{cn,ij}} = -\left(\kappa_{n,i}\delta_{n,ij}\right)\mathbf{n_i} \tag{3}$$

$$\mathbf{f_{ct,ij}} = -\left(\kappa_{t,i}\delta_{t,ij}\right)\mathbf{t_i} \tag{4}$$

$$\mathbf{f_{dn,ij}} = -\eta_{n,i}(v_\mathrm{r} \cdot \mathbf{n_i})\mathbf{n_i} \tag{5}$$

$$\mathbf{f_{dt,ij}} = -\eta_{t,i}\left\{(v_\mathbf{r} \cdot \mathbf{t_i})\mathbf{t_i} + \left(\omega_\mathbf{i} \times \mathbf{R_i} - \omega_\mathbf{j} \times \mathbf{R_j}\right)\right\} \tag{6}$$

where $\kappa_{n,i}$, $\delta_{n,ij}$, $\mathbf{n_i}$, $\eta_{n,i}$ and $\kappa_{t,i}$, $\delta_{t,ij}$, $\mathbf{t_i}$, $\eta_{t,i}$ are the spring constants, displacements between particles, unit vectors and viscous contact damping coefficients in the normal and tangential directions, respectively, v_r is the relative velocity between particles and $\mathbf{R_i}$ and $\mathbf{R_j}$ are the radii of particles

i and **j**, respectively. If $|\mathbf{f_{ct,ij}}| > |\mathbf{f_{cn,ij}}|\tan\phi$, then $|\mathbf{f_{ct,ij}}| = |\mathbf{f_{cn,ij}}|\tan\phi$, where tan ϕ is analogous to the coefficient of friction.

Computational fluid dynamics

The governing equations for describing the motion of the continuum gas phase are basically the Navier–Stokes equations. An additional source term in the momentum equation has been included to account for interphase interactions

$$\frac{\partial \varepsilon}{\partial t} + \nabla \cdot (\varepsilon \mathbf{u}) = 0 \tag{7}$$

$$\frac{\partial (\rho_f \varepsilon \mathbf{u})}{\partial t} + \nabla \cdot (\rho_f \varepsilon \mathbf{u}\mathbf{u}) = -\varepsilon \nabla P + \nabla \cdot (\mu_f \varepsilon \nabla \mathbf{u}) + \rho_f \varepsilon \mathbf{g} - \mathbf{F} \tag{8}$$

where **u** is the velocity vector, ρ_f is the fluid density, μ_f is the fluid viscosity, ε is the local average porosity, P is the fluid pressure and **F** is the source term due to fluid–particle interaction.

Fluid drag force

In a multiphase system, the interstitial fluid exerts drag forces on the solid particles whenever velocity differences exist between the two phases. Several fluid drag force models have been developed in the literature and the model due to Di Felice[32] which is applicable over a wide range of particle Reynolds numbers was used for calculating the fluid drag force in this study

$$\mathbf{f_{f,i}} = \mathbf{f_{f0,i}} \varepsilon_i^{-(\chi+1)} \tag{9}$$

$$\mathbf{f_{f0,i}} = 0.5 c_{d0,i} \rho_f \pi R_i^2 \varepsilon_i^2 |\mathbf{u_i} - \mathbf{v_i}| (\mathbf{u_i} - \mathbf{v_i}) \tag{10}$$

$$\chi = 3.7 - 0.65 \exp\left[-\frac{(1.5 - \log_{10} \mathrm{Re}_{p,i})^2}{2} \right] \tag{11}$$

$$c_{d0,i} = \left(0.63 + \frac{4.8}{\mathrm{Re}_{p,i}^{0.5}} \right)^2 \tag{12}$$

$$\mathrm{Re}_{p,i} = \frac{2 \rho_f R_i \varepsilon_i |\mathbf{u_i} - \mathbf{v_i}|}{\mu_f} \tag{13}$$

where $\mathbf{f_{f0,i}}$ is the fluid drag force on particle i in the absence of other particles, χ is an empirical parameter, ε_i is the local average porosity in the vicinity of particle i, $c_{d0,i}$ is the drag coefficient, $\mathrm{Re}_{p,i}$ is the Reynolds number based on particle diameter and $\mathbf{u_i}$ is the fluid velocity of the computational cell in which particle i is located.

Capillary liquid bridge force

Several models for describing the behavior of liquid bridges between solid particles have been reported in the literature. Simons et al.[33] obtained a closed form approximate solution of the Young–Laplace equation for calculating the rupture energy of pendular liquid bridges. In the current study, following Mikami et al.,[20] the capillary liquid bridge force between wet particles was calculated according to the following equations

$$\hat{\mathbf{f}}_{\mathbf{cap,ij}} = \exp\left(A \hat{h}_c + B\right) + C \tag{14}$$

For particle–particle capillary liquid bridge force

Table 1. Material Properties and System Parameters

Shape of Particles	Spherical
Number of particles	25,000
Particle diameter	1.0 mm
Particle density	2500 kg m^{-3}
Coefficient of restitution	0.9
Coefficient of friction	0.3
Gas density, ρ_f	1.205 kg·m^{-3}
Gas viscosity, μ_f	1.8×10^{-5} N s·m^{-2}
Gas velocity	1.0, 1.4, 1.6, and 1.8 m·s^{-1}
Dimensionless liquid volume, $\hat{V}$	0.01
Surface tension, γ	0.073 N·m^{-1}
Contact angle, θ	0 rad
System dimensions	64 mm length × 8 mm width × 800 mm height
Simulation time step	10^{-6} s

$$\hat{h}_c = (0.62\theta + 0.99)\hat{V}^{0.34} \tag{15}$$

$$A = -1.1\hat{V}^{-0.53} \tag{16}$$

$$B = \left(-0.34 \ln \hat{V} - 0.96\right)\theta^2 - 0.019 \ln \hat{V} + 0.48 \tag{17}$$

$$C = 0.0042 \ln \hat{V} + 0.078 \tag{18}$$

For particle–wall capillary liquid bridge force

$$\hat{h}_c = (0.22\theta + 0.95)\hat{V}^{0.32} \tag{19}$$

$$A = -1.9\hat{V}^{-0.51} \tag{20}$$

$$B = \left(-0.016 \ln \hat{V} - 0.76\right)\theta^2 - 0.12 \ln \hat{V} + 1.2 \tag{21}$$

$$C = 0.013 \ln \hat{V} + 0.18 \tag{22}$$

where $\hat{h}_c = h_c/R_i$, $\hat{V} = V/\pi R_i^3$, $\hat{\mathbf{f}}_{\mathbf{cap,ij}} = \mathbf{f_{cap,ij}}/\pi R_i \gamma$, h_c is the critical rupture distance between particles, V is the liquid bridge volume, γ is the surface tension, and θ is the contact angle. Ennis et al.[34] showed that viscous effects dominated the capillary liquid bridge force when the capillary number, Ca, was greater than 1 and surface tension dominated it when Ca was less than 0.001. It was assumed that the viscous contribution to the strength of the capillary liquid bridge force was negligible for the physical conditions applied in this study. This assumption could be evaluated by examining the capillary number which is the ratio of the dynamic to static force, $\mathrm{Ca} = \mu v_r/\gamma$, where μ is the liquid viscosity, v_r is the relative velocity between two particles connected by a liquid bridge and γ is the surface tension of the liquid. In the present study, the liquid was assumed to be water and relative velocities between particles were not expected to be greater than 1 m/s for the operating conditions applied. Thus, the capillary number was expected to be less than about 0.01 which supports the assumption that the contribution of viscous effects to the capillary liquid bridge force could be deemed negligible compared to that of surface tension.

Simulation conditions

The geometry of the computational domain considered in this study was a fluidized bed with a rectangular base measuring 64 mm × 8 mm and height of 800 mm. The granular materials consisted of 25,000 spherical particles with diameter 1.0 mm and density 2500 kg·m^{-3}. Other pertinent

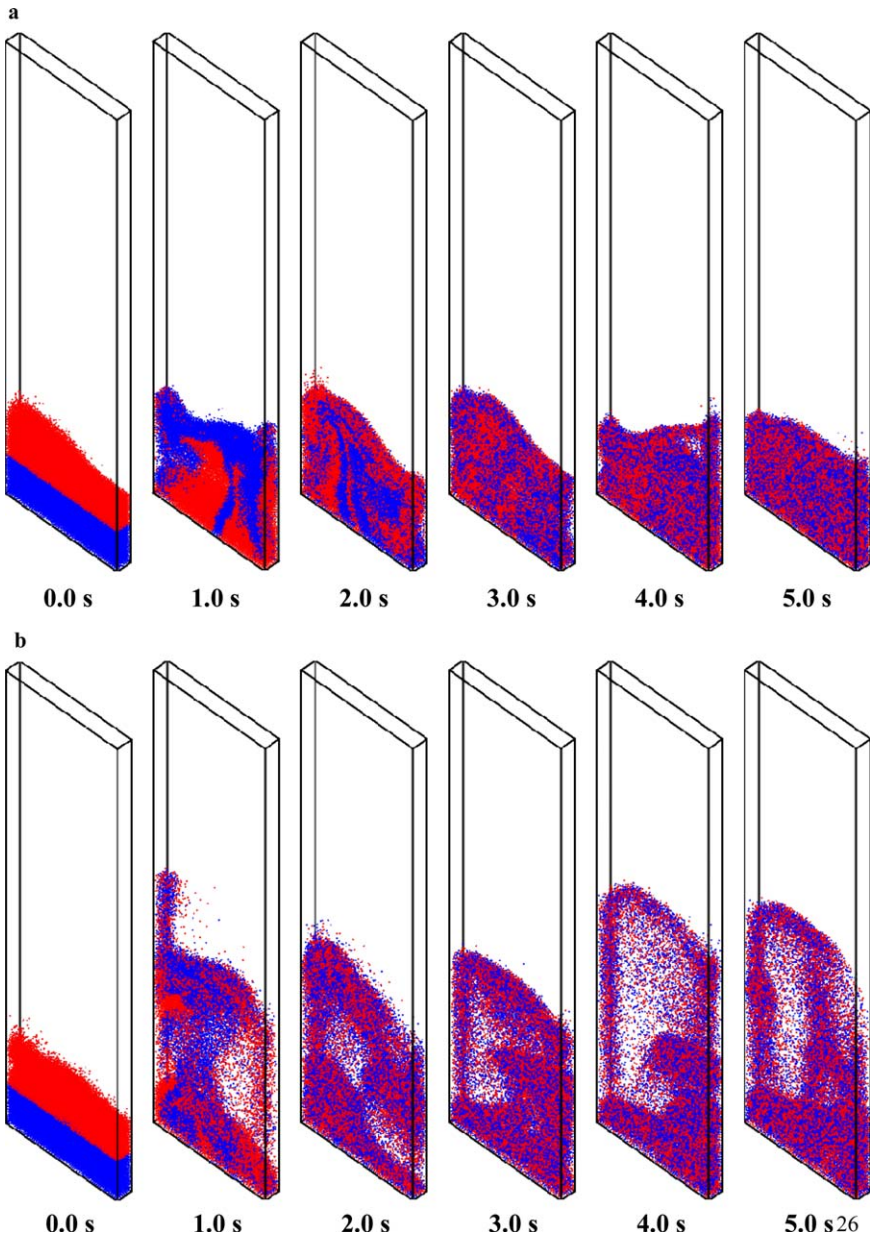

Figure 1. Mixing behaviors of dry particles in a gas fluidized bed.

The relative fluidizing velocities applied, $U/U_{mf,dry}$, were (a) 1.0 and (b) 1.8, where the minimum fluidization velocity, $U_{mf,dry}$, was approximately 1.0 m·s^{-1}. [Color figure can be viewed in the online issue, which is available at wileyonlinelibrary.com]

simulation parameters are presented in Table 1. In all simulations performed, particles were first allowed to settle freely under gravity for 0.5 s and form a packing at the bottom of the container before fluidizing air was initiated. A uniform fluidizing gas velocity was applied at the base of the computational domain to simulate a uniform gas distribution. Simulations were performed in three dimensions for both solid and gas phases.

Results and Discussion

Figure 1 shows the mixing behaviors of dry particles during fluidization at various fluidizing velocities. All fluidized bed systems contained equal amounts of monodispersed particles with identical physical properties. The packed beds formed at the start of each fluidization process were divided into two layers containing approximately equal numbers of particles, and particles in the two layers were colored differently to allow visualization of the subsequent mixing behaviors. With a low fluidizing velocity of 1.0 m·s^{-1}, the initial packed bed of particles was expanded only slightly (Figure 1a) corresponding to the state of incipient fluidization. The minimum fluidization velocity, $U_{mf,dry}$, of the packed bed was thus approximately 1.0 m·s^{-1}. Although particles were not lifted high from their original positions, they were nevertheless able to undergo vigorous relative motions within the slightly expanded bed giving rise to gradual mixing between the two layers of particles. Based on visual inspection, Figure 1a shows that the bed had become fairly well mixed at the end of 5 s. With a higher relative fluidizing velocity of $U/U_{mf,dry} = 1.4$, greater expansions of the bed and more vigorous relative motions of particles were observed (figure not shown for brevity). Consequently, the time required for the bed to become well mixed based on

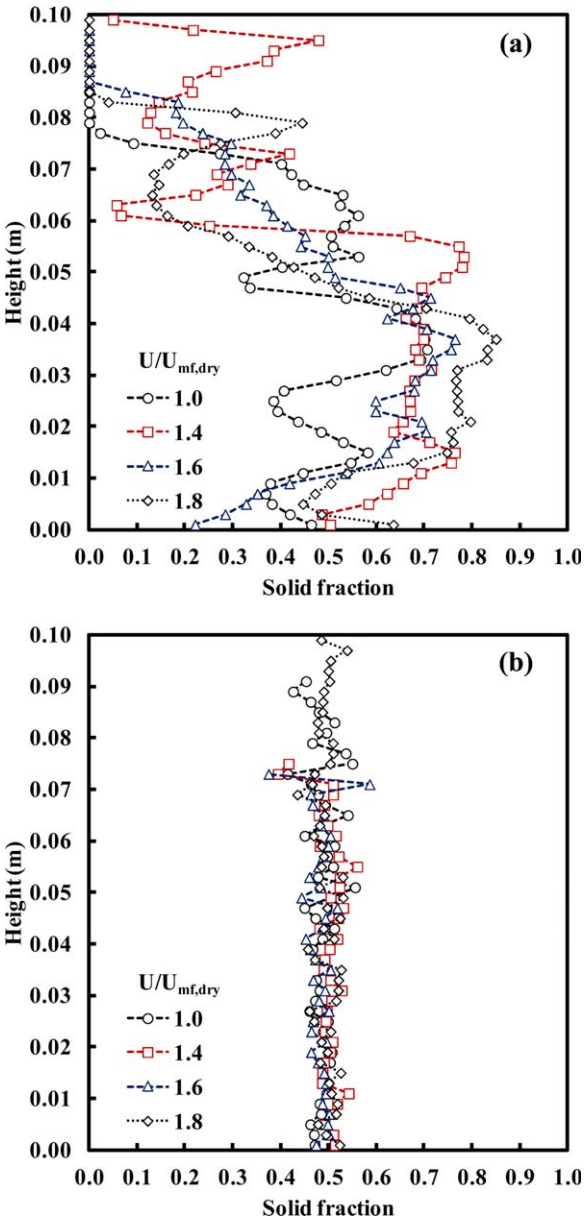

Figure 2. Distributions of spatially averaged fractions of particles originally belonging to the bottom layer of the packed beds of dry particles.

(a) 0.5 s and (b) 10 s after the start of the fluidization process. [Color figure can be viewed in the online issue, which is available at wileyonlinelibrary.com]

visual inspection was reduced to about 2 s. Similar observations may be made with the application of higher relative fluidizing velocities of $U/U_{mf,dry} = 1.6$ and 1.8 (Figure 1b).

The mixing behaviors of the various fluidized bed systems will now be examined more quantitatively by analyzing the variation of distribution of particles as well as a mixing index with time during the fluidization process. Figure 2a shows the spatially averaged fractions of particles originally belonging to the bottom layer of the packed bed as a function of position in the vertical direction 0.5 s after the start of the fluidization process. Consistent with the observations derived from Figure 1 previously, only a limited extent of mixing between the two layers of particles were achieved at 0.5 s for all fluidizing velocities investigated. The bottom sections of the fluidized beds still consisted of particles that originally belonged to the bottom layer of the packed bed at 0.5 s (Figure 2a). In contrast, Figure 2b shows that the fractions of these particles became approximately 0.5 throughout the entire bed after 10 s of fluidization for all fluidizing velocities investigated, indicating that almost perfect mixing between the original layers of particles had been achieved.

The progressions in time of the extents of mixing for the above fluidized bed systems may also be analyzed based on a mixing index.[1,2,35] Here, the Lacey mixing index was calculated at equal time intervals during the fluidization process for each fluidized bed system according to the following formula

$$\text{Lacey } index = \frac{\sigma_o^2 - \sigma}{\sigma_o^2 - \sigma_R^2} \tag{23}$$

where ${\sigma_o}^2$ and ${\sigma_R}^2$ are the theoretical upper and lower limits of mixture variances calculated as ${\sigma_o}^2 = p(1-p)$ and ${\sigma_R}^2 = p(1-p)/n$, p and $(1-p)$ are the proportions of the two groups of particles determined from samples, respectively, and n is the number of particles in each sample. The computational domain was divided into sampling cells with dimensions $4\,\text{mm} \times 4\,\text{mm} \times 4\,\text{mm}$ for sampling. Sampling was performed on every cell at equal time intervals and only samples containing at least 40 particles were used for calculating the Lacey mixing index. This was deemed representative of the state of mixing of the fluidized bed.

Figure 3 shows that the Lacey index for the fluidized bed system with an applied relative fluidizing velocity of $U/U_{mf,dry} = 1.0$ increased fairly rapidly from 0.0 to 1.0 within about 5 s, which was in agreement with the observation derived based on visual inspection of Figure 1a. With higher relative fluidizing velocities of 1.4, 1.6, and 1.8, the Lacey indices increased rapidly and reached 1.0 within about 2 s, indicating shorter times required to attain almost perfect

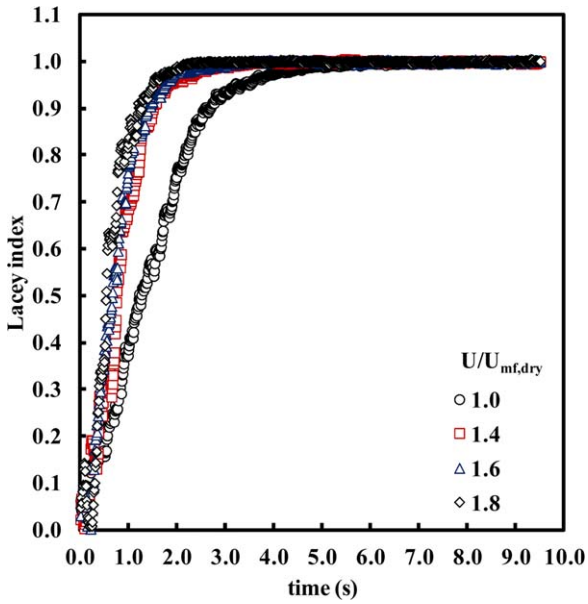

Figure 3. Time evolution of Lacey mixing indices for the fluidized bed systems containing dry particles at various relative fluidizing velocities.

[Color figure can be viewed in the online issue, which is available at wileyonlinelibrary.com]

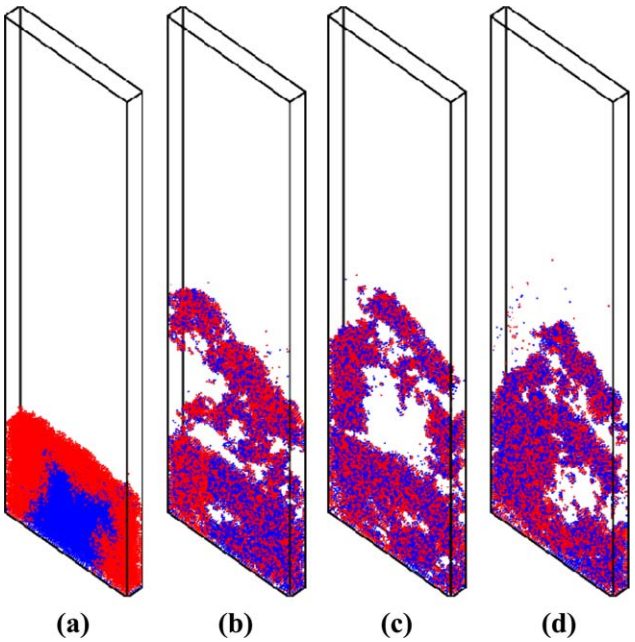

Figure 4. Mixing behaviors of wet particles in a gas fluidized bed.

The relative fluidizing velocities applied, $U/U_{mf,wet}$, were (a) 0.9, (b) 1.3, (c) 1.5, and (d) 1.6, where the minimum fluidization velocity, $U_{mf,wet}$, was approximately 1.1 $m \cdot s^{-1}$. [Color figure can be viewed in the online issue, which is available at wileyonlinelibrary.com]

mixing and thus higher mixing efficiencies at these fluidizing velocities. Interestingly, mixing efficiencies increased only minimally when relative fluidizing velocity was increased from 1.4 to 1.8. The mechanistic behaviors of the fluidized beds at the individual particle level giving rise to these macroscopic observations will be analyzed in greater details in a later section of this article after discussions of the mixing behaviors of fluidized bed systems containing wet solid particles.

Figure 4 shows the mixing behaviors of wet particles during fluidization at the relative gas velocities of $U/U_{mf,wet} =$ 0.9, 1.3, 1.5, and 1.6, where the minimum fluidization velocity, $U_{mf,wet}$, was determined to be approximately 1.1 $m \cdot s^{-1}$. Following Mikami et al.,[20] the amount of liquid present between particles was simulated to be 0.27 wt % for all cases considered in this study. The liquid content was assumed to remain constant throughout the fluidization and mixing process regardless of the fluidizing velocity applied. It may be observed that particle motions within the fluidized bed were significantly hindered by the presence of cohesive forces resulting from the wetness of particles. At the lowest relative gas velocity of $U/U_{mf,wet} = 0.9$, minimal expansion of the bed was observed and the two layers of particles in the original packed bed remained segregated as two large clusters even after 5 s of fluidization (Figure 4a). At higher relative fluidizing velocities, particles were observed to be fluidized in the form of large aggregates due to the presence of strong cohesive forces and fairly good mixing could be achieved after 5 s of fluidization (Figures 4b–4d). Although the formation of aggregates observed here resulted from the effects of wetness, the fluidization behaviors exhibited by the various fluidized bed systems were reminiscent of those of Geldart group C particles. Due to strong cohesive forces between adjacent particles, relative motions between particles that were essential for mixing to occur were severely hindered especially at low fluidizing velocities.

Figure 5a shows that the fluidized bed with an applied relative gas velocity of $U/U_{mf,wet} = 0.9$ was still in a state of almost complete segregation at 0.5 s, in agreement with the qualitative observations made earlier. At higher relative fluidizing velocities, although mixing between the two layers of particles had begun at 0.5 s, large extents of segregation could still be discerned based on the solid fraction distributions. Figure 5b shows that mixing was essentially complete after 10 s of fluidization at the relative velocities of 1.3, 1.5, and 1.6 as exhibited by more or less uniform distributions of

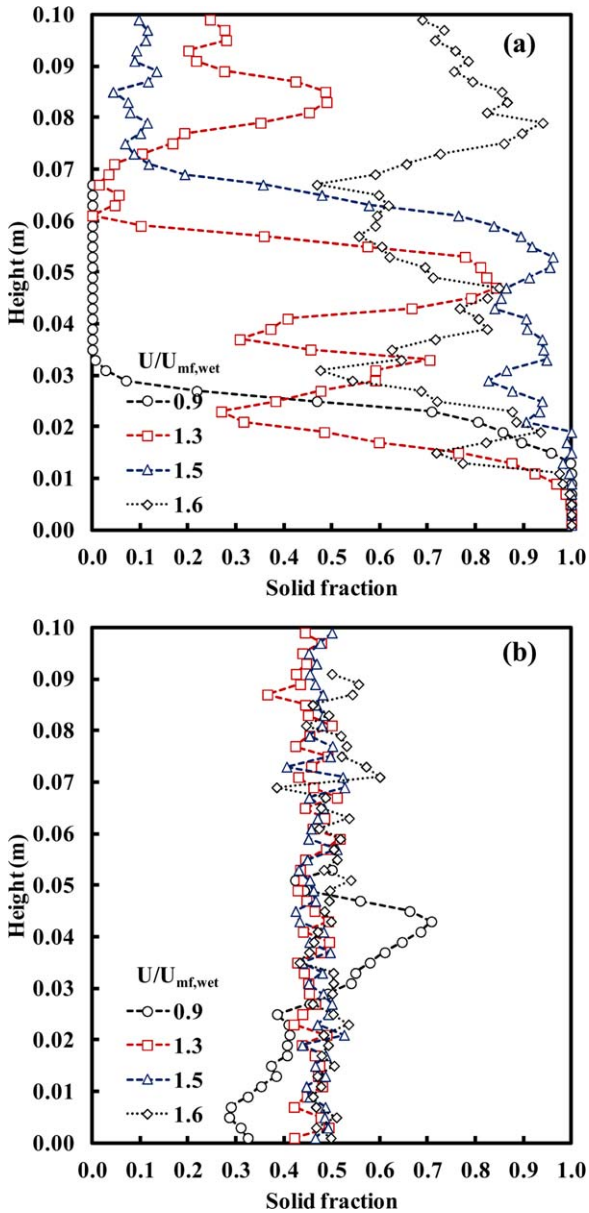

Figure 5. Distributions of spatially averaged fractions of particles originally belonging to the bottom layer of the packed beds of wet particles.

(a) 0.5 s and (b) 10 s after the start of the fluidization process. [Color figure can be viewed in the online issue, which is available at wileyonlinelibrary.com]

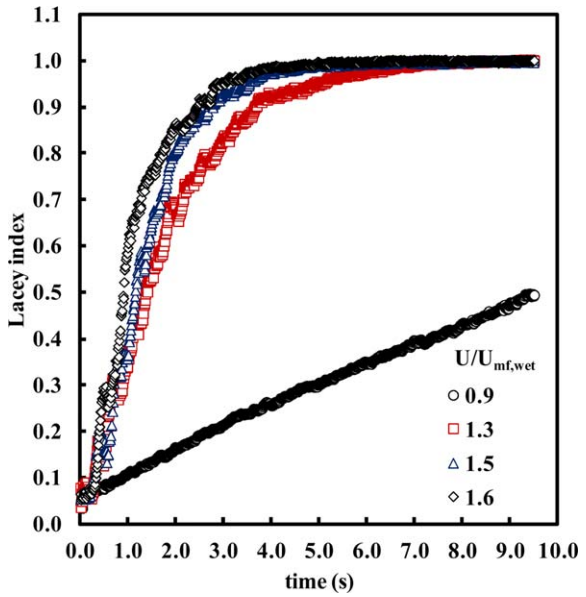

Figure 6. Time evolution of Lacey mixing indices for the fluidized bed systems containing wet particles at various relative fluidizing velocities.

[Color figure can be viewed in the online issue, which is available at wileyonlinelibrary.com]

solid fraction throughout the entire beds. In contrast, a non-uniform solid fraction distribution indicating some extent of segregation between the original layers of particles was still discernable for the case of fluidization at $U/U_{mf,wet} = 0.9$.

The lower mixing efficiencies of wet particles during fluidization may be observed from the Lacey index profiles and comparisons with those presented earlier for dry particles. It may be seen from Figure 6 that the Lacey index for the fluidized bed system with an applied relative gas velocity of $U/U_{mf,wet} = 0.9$ increased much more slowly than those seen in Figure 3 for dry particles and reached a value of 0.5 after 10 s. In other words, mixing was still very far from complete after 10 s of fluidization and this was consistent with the qualitative observations made earlier based on visual inspection of Figure 4a. Figure 6 also shows that, in contrast with the profiles for dry particles, the Lacey index profiles obtained at higher relative fluidizing velocities of 1.3, 1.5, and 1.6 do not collapse onto one another and the rate of increase of Lacey index values increased with increasing fluidizing velocity. The time required for the Lacey index to reach a value of 1.0 decreased from about 7 to 5 and to 4 s as relative fluidizing velocity increased from 1.3 to 1.5 and to 1.6. In comparison with the case of fluidization of dry particles at the relative fluidizing velocity of 1.6 where the time required for the Lacey index to reach a value of 1.0 was observed to be about 2 s, that required for the case of fluidization of wet particles at the same relative fluidizing velocity was about twice as long. This may indicate that the fluidizing velocity had become a limiting factor that determined the mixing efficiencies of the fluidized bed systems containing wet solid particles which was in complete contrast to the case of dry particles. Here, high relative fluidizing velocity was necessary and essential for particles to be able to overcome the strong cohesive forces arising from wetness which was in turn required for particles to be able to undergo relative motions and thus mixing. As such, mixing efficiencies could be increased by increasing fluidizing velocity in this latter case. In the remaining sections of this article, detailed mechanistic behaviors at the individual particle scale will be analyzed in relation with dynamic force data to substantiate the above explanations with a view towards achieving deeper insights to the mixing mechanisms associated with wet particles in fluidized bed systems.

Figure 7 shows typical snapshots of the fluidized bed systems containing dry particles at various fluidizing velocities. Only a region that is one particle diameter in thickness extracted from the midplane of the bed along the spanwise direction is presented to aid visualization of particle behaviors within the interior of the bed. One apparent feature of fluidization of dry particles at the operating conditions investigated here is the formation of large bubbles. During the fluidization process, individual particles may be randomly

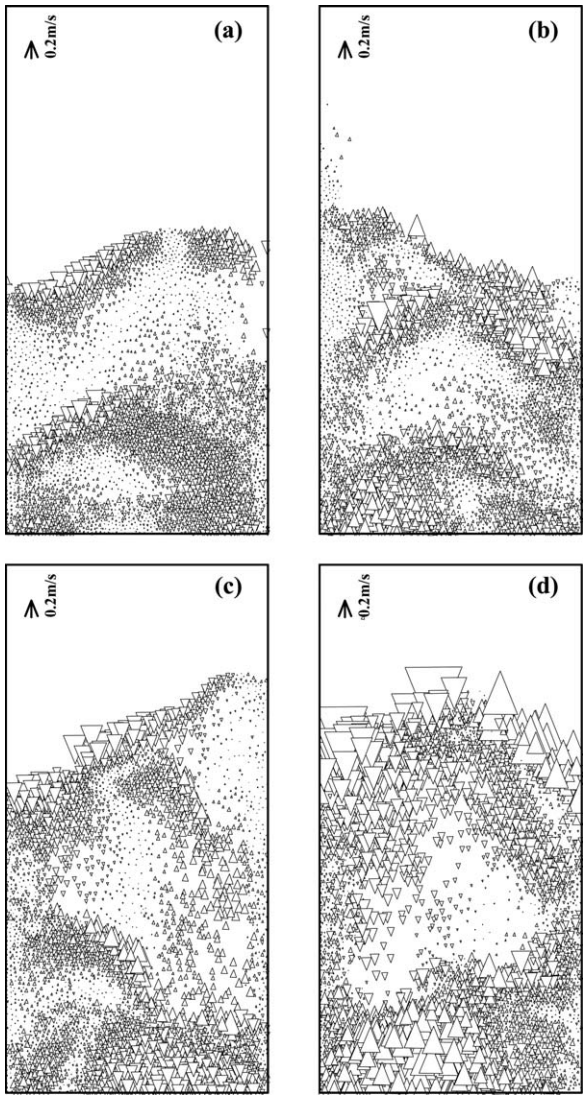

Figure 7. Velocity vectors of particles located within a region that is one particle diameter in thickness extracted from the midplane of the bed along the spanwise direction for the fluidized bed systems containing dry particles at relative fluidizing velocities, $U/U_{mf,dry}$, of (a) 1.0, (b) 1.4, (c) 1.6, and (d) 1.8.

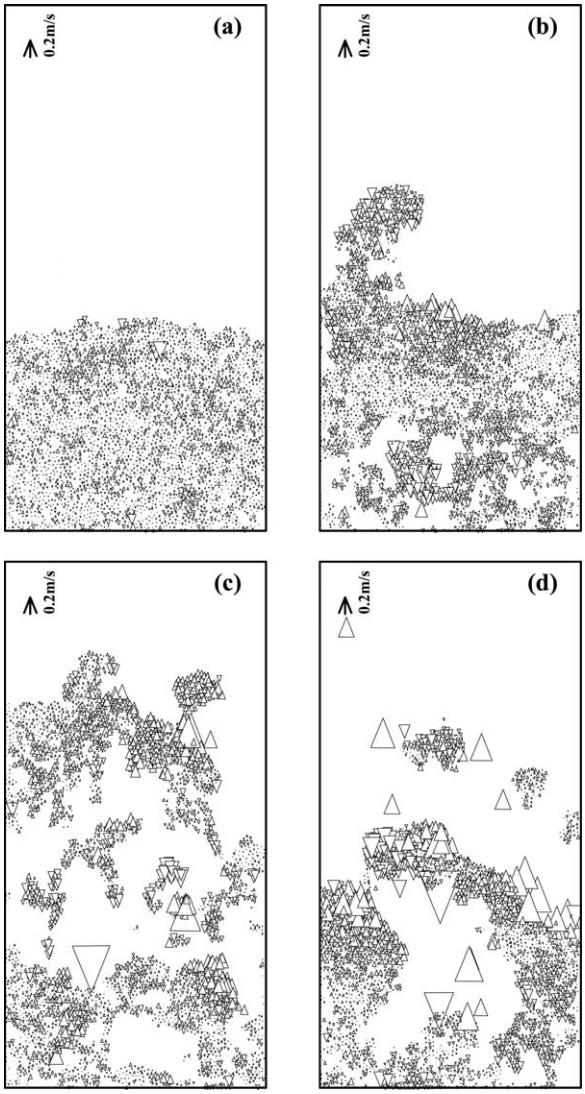

Figure 8. Velocity vectors of particles located within a region that is one particle diameter in thickness extracted from the midplane of the bed along the spanwise direction for the fluidized bed systems containing wet particles at relative fluidizing velocities, $U/U_{mf,wet}$, of (a) 0.9, (b) 1.3, (c) 1.5, and (d) 1.6.

transported into either the lean bubble phase or rich emulsion phase. In addition, the particle velocity vectors presented in Figure 7 indicate that most particles were capable of unhindered, independent motions. Although bulk movements of particles dictated by the gas flow resulted in some extent of synchronized solid motions, relative movements between individual particles that promoted mixing were also observed. In contrast, Figure 8 shows that wet particles moved in the form of large aggregates or clusters during fluidization as described earlier. Due to the presence of strong cohesive forces that hindered relative motions between adjacent particles, particles within each aggregate tended to exhibit synchronized motions as a group. In the absence of slip between individual particles, mixing within each aggregate was hindered significantly. In this case, mixing may only occur more effectively at a larger scale between individual aggregates rather than at the individual particle scale. For the latter to occur, strong cohesive forces resulting from capillary effects between wet particles needed to be overcome by fluid drag forces or collision forces that arise during particle–particle collisions. This would then allow particles originally belonging to a particular aggregate to be dislodged from the aggregate and become an independent particle before joining another aggregate. Such exchange of particles between aggregates was the basis of the mixing process that occurred during fluidization of wet particles.

Figure 9 shows the time evolution of the various types of forces experienced by every particle in the fluidized bed. The magnitude of each force was calculated by averaging over all particles in the entire bed and nondimensionalizing by the particle weight. It may be observed that the conditions required for mixing to occur during fluidization of wet particles as described above were fairly difficult to achieve under the operating conditions imposed. For all fluidizing velocities applied, the average fluid drag force was much smaller than the cohesive capillary liquid bridge force experienced by each particle in the fluidized bed while particle–particle contact forces were on average slightly stronger than capillary forces. Capillary and collision forces were the dominant forces present in such fluidized bed systems and it might be expected that the basic condition required for mixing to occur, whereby fluid drag forces or collision forces overcome capillary forces acting on each particle, was difficult to satisfy on average. This explains the lower mixing efficiencies observed with such fluidized bed systems in comparison with those containing dry particles. With the application of higher fluidizing velocities, larger fluctuations in average fluid drag forces and collision forces may improve the likelihood of such forces overcoming capillary forces for specific particles within the system. This implies that fluidization velocity was indeed the limiting factor for the operating conditions applied that determined the efficiencies with which mixing could occur and, thus, explains the improvements in rates of increase in Lacey index values observed with increasing fluidizing velocities seen earlier in Figure 6. To our knowledge, this is the first mechanistic explanation of macroscopic mixing behaviors of wet particles in fluidized bed systems via a dynamic force analysis at the individual particle length scale.

Conclusions

The mixing behaviors of wet granular materials in gas fluidized bed systems were investigated computationally in this study. The conventional CFD–DEM model was coupled with a capillary liquid bridge force model and used for simulations of fluidization of dry and wet solid particles at various fluidizing velocities. The mixing efficiencies of wet particles were observed to be lower than those of dry particles. Due to the presence of cohesive forces between wet particles arising from the formation of capillary liquid bridges, relative motions between adjacent particles were hindered significantly. Consequently, wet particles were observed to be fluidized in the form of aggregates or clusters. Within each cluster, independent motions of individual particles relative to one another that were important for mixing to occur were limited. Mixing thus occurred at the length scales of aggregates rather than those of particles. Based on detailed analyses of dynamic force data extracted from the simulations conducted, capillary liquid bridge forces between particles during the fluidization process were indeed observed to be

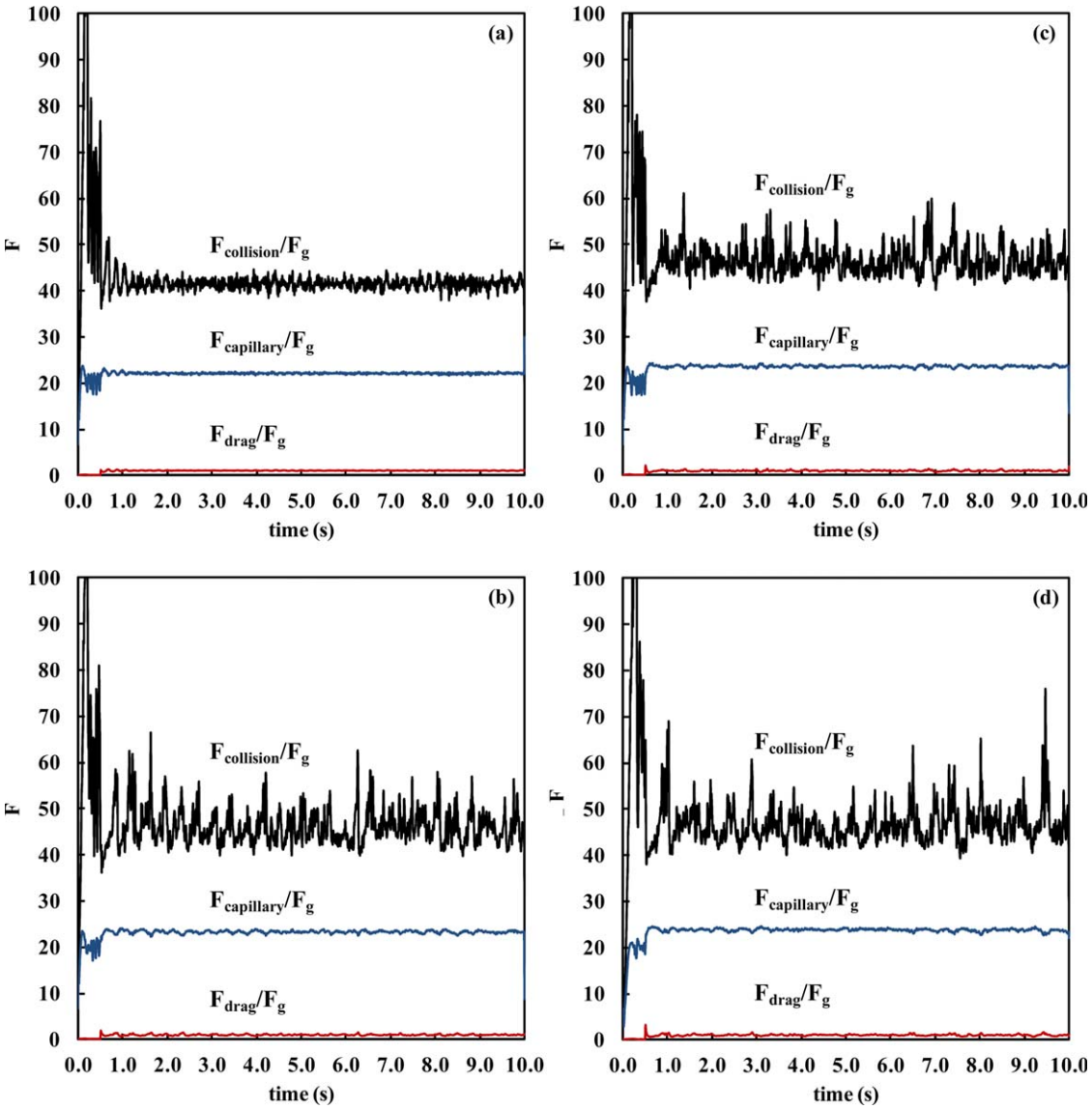

Figure 9. Time evolution of average relative capillary liquid bridge forces ($F_{capillary}/F_g$), relative fluid drag forces (F_{drag}/F_g), and relative particle–particle collision forces ($F_{collision}/F_g$) for the fluidized bed systems containing wet particles at relative fluidizing velocities, $U/U_{mf,wet}$, of (a) 0.9, (b) 1.3, (c) 1.5, and (d) 1.6, where F_g is particle weight.

[Color figure can be viewed in the online issue, which is available at wileyonlinelibrary.com]

stronger on average than both fluid drag forces and particle–particle collision forces. This explained the difficulty with which particles could be removed from a particular aggregate and transferred onto a different aggregate. Such particle transfers necessarily required strong capillary forces to be overcome by drag or collision forces and were essential for mixing at the individual particle length scale to be achieved. It would be pertinent to extend the present study towards detailed parametric analyses of various factors such as moisture content of the fluidized beds containing wet particles, material properties of the granular materials and modes of gas injection on mixing efficiencies. The mixing or segregation behaviors of binary mixtures of wet granular materials with different sizes or densities may also be investigated with the modified CFD–DEM model applied in this study. It may also be interesting to carry out integrated mixing–drying simulations of gas fluidized bed systems by further coupling the current computational model with an appropriate solids drying model. In the research literature, studies of mixing and segregation behaviors of wet or cohesive particles in various types of systems have been reported. Li and McCarthy[36] developed phase diagrams for mixing and segregation of cohesive particles in rotating drums and annular shear cells.[37] It is envisaged that such phase diagrams can also be developed for mixing of wet particles in gas fluidized bed systems in a future study.

Acknowledgment

This study has been supported by the Economic Development Board (EDB) of Singapore through the Minerals, Metals, and Materials Technology Center (M3TC) of the National University of Singapore (NUS) under grant number R-261–501-017–414.

Literature Cited

1. Rhodes MJ, Wang XS, Nguyen M, Stewart P, Liffman K. Study of mixing in gas-fluidized beds using a DEM model. *Chem Eng Sci*. 2001;56:2859–2866.
2. Feng YQ, Xu BH, Zhang SJ, Yu AB. Discrete particle simulation of gas fluidization of particle mixtures. *AIChE J*. 2004;50:1713–1728.
3. Feng YQ, Yu AB. Microdynamic modeling and analysis of the mixing and segregation of binary mixtures of particles in gas fluidization. *Chem Eng Sci*. 2007;62:256–268.
4. Dahl SR, Hrenya CM. Size segregation in gas-solid fluidized beds with continuous size distributions. *Chem Eng Sci*. 2005;60:6658–6673.
5. Chaikittisilp W, Taenumtrakul T, Boonsuwan P, Tanthapanichakoon W, Charinpanitkul T. Analysis of solid particle mixing in inclined fluidized beds using DEM simulation. *Chem Eng J*. 2006;122:21–29.
6. Nakamura H, Tokuda T, Iwasaki T, Watano S. Numerical analysis of particle mixing in a rotating fluidized bed. *Chem Eng Sci*. 2007; 62:3043–3056.
7. Cooper S, Coronella CJ. CFD simulations of particle mixing in a binary fluidized bed. *Powder Tech*. 2005;151:27–36.
8. Huilin L, Yunhua Z, Ding J, Gidaspow D, Wei L. Investigation of mixing/segregation of mixture particles in gas-solid fluidized beds. *Chem Eng Sci*. 2007;62:301–317.
9. Mazzei L, Casillo A, Lettieri P, Salatino P. CFD simulations of segregating fluidized bidisperse mixtures of particles differing size. *Chem Eng J*. 2010;156:432–445.
10. Azizi S, Hosseini SH, Ahmadi G, Moraveji M. Numerical simulation of particle segregation in bubbling gas-fluidized beds. *Chem Eng Tech*. 2010;33:421–432.
11. Coroneo M, Mazzei L, Lettieri P, Paglianti A, Montante G. CFD prediction of segregating fluidized bidispersed mixtures of particles differing in size and density in gas–solid fluidized beds. *Chem Eng Sci*. 2011;66:2317–2327.
12. Gui N, Fan J. Numerical study of particle mixing in bubbling fluidized beds based on fractal and entropy analysis. *Chem Eng Sci*. 2011;66:2788–2797.
13. Du B, Fan LS, Wei F, Warsito W. Gas and solids mixing in a turbulent fluidized bed. *AIChE J*. 2002;48:1896–1909.
14. Wormsbecker M, Adams A, Pugsley T, Winters C. Segregation by size difference in a conical fluidized bed of pharmaceutical granulate. *Powder Tech*. 2005;153:72–80.
15. Joseph GG, Leboreiro J, Hrenya CM, Stevens AR. Experimental segregation profiles in bubbling gas-fluidized beds. *AIChE J*. 2007;53: 2804–2813.
16. Zhong W, Zhang M, Jin B, Zhang Y, Xiao R, Huang Y. Experimental investigation of particle mixing behavior in a large spout-fluid bed. *Chem Eng Proc*. 2007;46:990–995.
17. Huang C, Wang Y, Wei F. Solids mixing behavior in a nano-agglomerate fluidized bed. *Powder Tech*. 2008;182:334–341.
18. Zhang Y, Jin B, Zhong W. Experimental investigation on mixing and segregation behavior of biomass particle in fluidized bed. *Chem Eng Proc*. 2009;48:745–754.
19. Chew JW, Wolz JR, Hrenya CM. Axial segregation in bubbling gas-fluidized beds with Gaussian and lognormal distributions of Geldart group B particles. *AIChE J*. 2010;56:3049–3061.
20. Mikami T, Kamiya H, Horio M. Numerical simulation of cohesive powder behavior in a fluidized bed. *Chem Eng Sci*. 1998;53: 1927–1940.
21. Jain K, Shi D, McCarthy JJ. Discrete characterization of cohesion in gas-solid flows. *Powder Tech*. 2004;146:160–167.
22. Tardos G, Pfeffer R. Chemical reaction induced agglomeration and defluidization of fluidized beds. *Powder Tech*. 1995;85:29–35.
23. Wormsbecker M, Pugsley T. The influence of moisture on the fluidization behaviour of porous pharmaceutical granule. *Chem Eng Sci*. 2008;63:4063–4069.
24. Cundall PA, Strack ODL. A discrete numerical model for granular assemblies. *Geotechnique*. 1979;29:47–65.
25. Lim EWC. Voidage waves in hydraulic conveying through narrow pipes. *Chem Eng Sci*. 2007;62:4529–4543.
26. Lim EWC. Master curve for the discrete-element method. *Ind Eng Chem Res*. 2008;47:481–485.
27. Lim EWC. Vibrated granular bed on a bumpy surface. *Phys Rev E*. 2009;79:041302.
28. Lim EWC. Density segregation in vibrated granular beds with bumpy surfaces. *AIChE J*. 2010;56:2588–2597.
29. Lim EWC. Granular Leidenfrost effect in vibrated beds with bumpy surfaces. *Eur Phys J E Soft Matter*. 2010;32:365–375.
30. Lim EWC, Yao J, Zhao YL. Pneumatic transport of granular materials with electrostatic effects. *AIChE J*. 2012;58:1040–1059.
31. Lim EWC, Feng R. Agglomeration of magnetic nanoparticles. *J Chem Phys*. 2012;136:124109.
32. Di Felice R. The voidage function for fluid-particle interaction systems. *Int J Multiphase Flow*. 1994;20:153–159.
33. Simons SJR, Seville JPK, Adams MJ. An analysis of the rupture energy of pendular liquid bridges. *Chem Eng Sci*. 1994;49: 2331–2339.
34. Ennis BJ, Li J, Tardos GI, Pfeffer R. The influence of viscosity on the strength of an axially strained pendular liquid bridge. *Chem Eng Sci*. 1990;45:3071–3088.
35. Chandratilleke GR, Zhou YC, Yu AB, Bridgwater J. Effect of blade speed on granular flow and mixing in a cylindrical mixer. *Ind Eng Chem Res*. 2010;49:5467–5478.
36. Li HM, McCarthy JJ. Controlling cohesive particle mixing and segregation. *Phy Rev Lett*. 2003;90:184301.
37. Li HM, McCarthy JJ. Cohesive particle mixing and segregation under shear. *Powder Tech*. 2006;164:58–64.

Manuscript received Aug. 1, 2012, and revision received Jun. 1, 2013.